Maximizing stoichiometry control in reactive sputter deposition of TiO_2

Brian D. Hoskins[a)]
Materials Department, University of California Santa Barbara, Santa Barbara, California 93106

Dmitri B. Strukov
Electrical and Computer Engineering Department, University of California Santa Barbara, Santa Barbara, California 93106

(Received 25 October 2016; accepted 4 January 2017; published 24 January 2017)

Thin films of amorphous TiO_2 are grown by direct current (DC) reactive magnetron sputtering. Using modern models of DC reactive sputtering, conditions were established to maximize control of the O:Ti ratio by indirectly monitoring the change in ion-induced secondary electron emission of the Ti target. The Ti resistivity was continuously varied through over 12 orders of magnitude, and changes in stoichiometry were observed by Rutherford backscattering. Combining observed changes in stoichiometry with a predictive model of the composition, a percolative transition could be observed exhibiting universal and nonuniversal scaling parameters. © *2017 American Vacuum Society*.
[http://dx.doi.org/10.1116/1.4974140]

I. INTRODUCTION

Reactive sputter deposition of TiO_2 films has been extensively studied over the years with a particular emphasis on growth rates. Emerging technologies, in particular, resistive random access memory or memristors based on TiO_x, have no growth rate constraints but require a high degree of control over the departure from stoichiometry in order to maximize device performance. Models of reactive sputter deposition like the Berg Model,[1–4] which have historically been used to maximize growth rates,[3] can also be used to establish conditions for maximal control over the stoichiometry and can be implemented either with or without active feedback systems to defeat target poisoning.[5–7]

In the Berg model, maximal correspondence between theory and experiment will occur during conditions of perturbative oxygen flow, i.e., the reactive gas does not contribute substantially to the sputtering process other than to oxidize the target chemically. This can be established at relatively low powers and high fluxes of sputtering gas. Under these conditions, in the limiting case where gas absorption through fully oxidized regions of the film can be neglected, it can be shown (e.g., see Sec. I of supplementary material)[26] that the departure from stoichiometry will vary quadratically with the oxidation state of the target at small deviations as well as inversely with the collector:target ratio. Substantially reduced targets at great distances, therefore, can generate small deviations from stoichiometry in a controllable manner.

It is been experimentally verified that both the coefficient of ion-induced secondary electron emission (ISEE)[8–10] and sputter yield from suboxide targets vary linearly with the oxidation state of the target. Consequently, under conditions of perturbative oxygen flow, the ISEE can be indirectly measured *in situ* by monitoring the discharge voltage of the magnetron sputtering target or *ex situ* by measuring the Ti flux. Continuous control over both implies continuous control over the composition due to strong coupling between target and film oxidation.

a)Electronic mail: bhoskins@engineering.ucsb.edu

II. EXPERIMENT

All growths were carried out at room temperature in a custom built high vacuum sputter chamber pumped by a Cryotorr 800 with a 1000 l/s pump rate to a base pressure of 3×10^{-8} Torr. To pump out target hysteresis, all growths were conducted with the pump gate valve fully opened. Growths were conducted at an operating pressure of 600 μTorr induced by a flow rate of 190 sccm of 99.99% pure Ar. A 3-in. diameter Ti target (99.99% Kurt J Lesker) was used in a Mighty Mac sputter gun and operated at a sputtering power of 150 W for all growths. Continuous control over the discharge voltage was experimentally confirmed by varying the O_2 flow rate from 0 to 16 sccm (see supplementary material).

To control the oxidation state of the target, the relative change in the discharge voltage, or oxidation factor, for partial oxidation versus full oxidation was chosen as a state variable such that

$$V^* = \Delta V / \Delta V_{\max}. \tag{1}$$

For such a state variable, $V^* = 0$ should correspond to pure Ti in both the film and the target and $V^* = 1$ should correspond to TiO_2 in both the film and target, thereby representing a bounded domain over which to vary the thin film composition. Since these values are easily measured from the magnetron power supply, it becomes trivial to use a dimensionless state variable as a process control parameter allowing reproducible growth of reduced oxide films. Since V^* should depend only on the oxidation state of the target, provided the background concentration of oxygen is small enough, it can be a sensitive measure of the state of the target. Since the Berg model implies the geometry of the chamber (independent of other values such as the magnetron power which might vary ΔV and $\Delta V_{\max}$) determines the relationship between the target and the film oxidation, V^* can be a useful dimensionless variable to track the composition of the film by monitoring the state of the target.

Two growth series were conducted so as to characterize the control over the sputtering process. The first series was a

growth rate and resistivity series grown on quartz substrates. Interpolation was used to predict growth rates such that all films were grown to a thickness of 25–35 nm. Film thicknesses were determined from Fourier transform analysis used in the GXRR software package on x-ray reflectivity spectra acquired from an X'Pert Panalytical X-ray diffractometer grazing incidence X-ray diffractometry of these films (not shown) showed no crystalline structure. Ti/Pt contacts were deposited on the four corners of the films to for subsequent van der Pauw measurements at room temperature. The second series were precisely calibrated growths by X-ray reflectivity (XRR) of four different 100 nm thick films grown on CVD diamond substrates (Diamond Materials GmbH) for use in Rutherford backscattering analysis (RBS). Although RBS is a standardless technique, propagation of systematic error (by growing constant thicknesses) can push error down to counting statistics when calculating dimensionless quantities between spectra. Dimensionless quantities are independent of the values for the cross sections and stopping powers which are limited to only ~1% accuracy and ~0.1% accuracy, respectively.[11]

III. RESULTS AND DISCUSSION

Measurements of the Ti flux from series 2 (Fig. 1), from both RBS (oxide films) and XRR Ti (metal films), show linear modulation of the Ti flux with target oxidation factor over the entire range, demonstrating a successful transformation from a nonlinear (gas flow) to linear (Ti flux) independent variable. The values of the stoichiometry versus oxidation factor measured from RBS (Fig. 2) depended significantly on the modeling [RUMP (Ref. 12) and SIMNRA (Ref. 13)] method used with increasing accuracy with

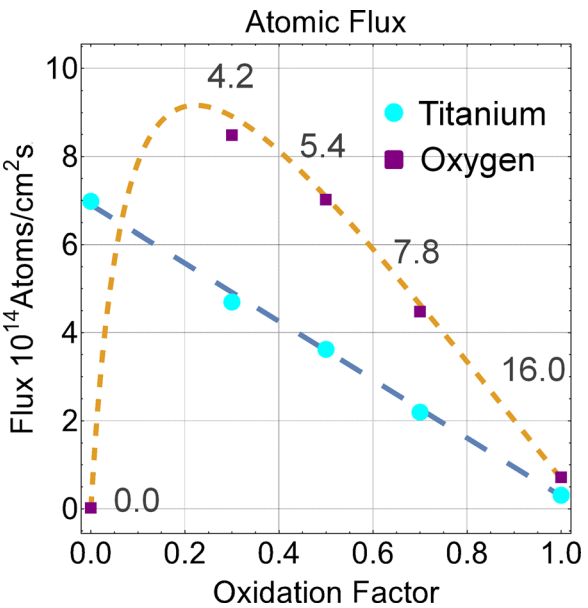

FIG. 1. (Color online) Atomic flux of titanium and incorporation rate of oxygen into the TiO_x films as measured by RBS. The values at oxidation factor 0 are calculated using XRR with the density of titanium and chamber base pressure estimate for oxygen. Numbers adjacent oxygen flux indicate associated flow rate in sccm. Note the decreasing oxygen incorporation despite increasing oxygen flow rate.

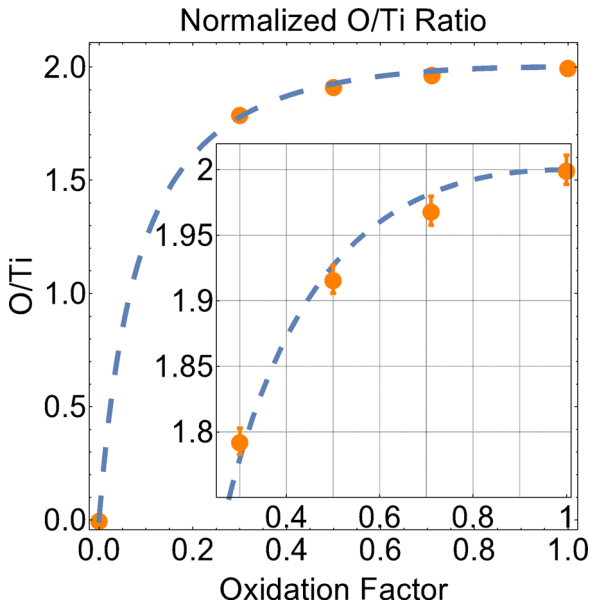

FIG. 2. (Color online) Normalized O/Ti ratio as measured by RBS. Error bars are 1-sigma from χ^2 reflecting experimental precision. Systematic error from uncertainty of the cross-section is neglected as common to all values. Value at 0 reflects composition of the target.

superior models, but the shape and precision of the curve depended purely on the ratio of total integrated charge as measured from the oxidation factor 1 regardless of the modeling method. From the χ^2 calculations in SIMNRA, the 1-sigma experimental precision (not accuracy) in the composition was approximately ±0.56%. Almost the entire range from 0.3 to 1.0 in the phase space is dominated by compositions consistent with rutile defect structures associated with Magnelli phases which are of the most engineering interest. Normalizing the compositions allows fitting of the simplified Berg model equation of state between target composition and film composition

$$x_f = \frac{2x_t}{x_t + \left(\frac{Y_{\text{oxide}}}{Y_{\text{metal}}}\right)(2 - x_t) + \left(\frac{Y_{\text{oxide}}}{Y_{\text{metal}}}\right)\left(\frac{A_f}{A_t}\right)\left(\frac{2 - x_t}{x_t}\right)}, \tag{2}$$

where Y_{oxide} and Y_{metal} are the sputter yield of Ti in oxide and metal. A_f and A_t are the effective film and target areas, respectively. x_t and x_f are the target and the film departures from stoichiometry. Since this model neglects higher order effects such as knock-in effects of reactive species into the target, it likely breaks down near the edges of the domain,[4,14] but this has not been extensively studied and few systems have observed such a strong linear correspondence between any state variable and the Ti-flux.

The oxidation factor is substituted for the actual film composition since it is empirically directly proportional to the Ti flux, the same condition existing between target composition and Ti flux in the Berg model. Using the extracted ratio of sputter yield from the Ti Flux curve $Y_{\text{oxide}}/Y_{\text{metal}} = 0.048$ an apparent collector:target area ratio of $A_f/A_t = 270.28$ is extracted by numerical fitting under the ∞-norm.

Four point probe measurements of the same films shows continuous modulation of the film resistivity and Seebeck coefficient through over 12 orders of magnitude as well as n-type conductivity (see supplementary material). Unfortunately, the resistivity values for oxidation factors greater than 0.71 could not be measured due to the high magnitude of the resistance. However, by combining the compositional equation of state with the resistivity data, functional relations between conductivity and composition can be extracted (Fig. 3). Immediately apparent from the log–log plot is the existence of two distinct regimes: a subthreshold and postcritical regime. In percolation theory, the conductivity is governed by[15]

$$\sigma_{\text{material}} = \sigma_0 (p - p_c)^t, \tag{3}$$

with t being the critical exponent for percolation as $p \to p_c$, with p_c being the critical concentration for percolation below which the film is insulating. For a metal-insulator transition driven by a defect band transition, t should be around 1 or sometimes $^1/_2$.[16] However, the simplest power law fit with $p_c = 0$ yields $t = 2.5$, and the curve can be exceptionally well fit with the strictly classical $t = 2$ seen in metal-insulator composites, a prefactor of $\sigma_o = 898\ \text{S m}^{-1}$, and a fit value of $p_c = 0.0125$, which is firmly in the transition region and half the observed deficiency of 0.023.[15] This suggests that the percolation is driven by bridging oxygen vacancies as opposed to an extended defect band—a fact not surprising given the amorphous nature of the films would suppress conductivity from free electrons.

More striking is the incredibly low value of p_c for such a classical transition. Continuum percolation models typically put the value of p_c near 0.5. However, the reduced value of p_c can be resolved taking into account the precise defect chemistry of aggregates of oxygen vacancies in TiO_2. Vacancies are known to condense in reduced rutile into shear planes with the thickness of half a lattice parameter and infinite diameter. Taking reduced rutile crystals to elevated temperature and quenching them results in incompletely grown shear planes randomly distributed with random diameters ranging from 20 to 30 Å to any size larger.[17–19] Percolation in TiO_2 is likely driven by the presence of very high aspect ratio structures which could be described by ellipsoids of thickness 4 Å and arbitrary major (b) and minor (a) axis. In the limiting case of highly oblate or prolate ellipsoids, the critical percolative concentration obeys the relation[20]

$$p_c \to \begin{cases} 0.6\dfrac{b}{a}, & \text{for prolate} \\ 1.27\dfrac{b}{a}, & \text{for oblate.} \end{cases} \tag{4}$$

Such a model would predict that the effective diameters of oblate disks is ~200 Å and the length of prolate needles is ~90 Å though there is likely a distribution running the range of these shapes. The percolative analysis suggests clusters ranging from ten to a couple thousand vacancies in the extreme prolate and oblate limits, respectively, determine the electrical resistivity. This simple analysis cannot account for the full range of more complex shapes with a nontrivial fractal dimension, but suggests that sufficiently high aspect ratio clusters can account for the observed percolation with moderate sizes.

The subthreshold and critical region conductivity is not so easily described, but this is a commonly observed effect.[21–23] This behavior is typically fit with an exponential and our exponential function provides a good fit to the data with prefactor 0.124 GSm^{-1} and dimensionless scaling factor of 624. The subthreshold conductivity is often attributed to hopping or tunneling transport between clusters, with increasing density of clusters leading to continuously enhanced conductivity.

The ability to finely tune the composition has interesting implications for resistive switching, since the controlled introduction of defects can likely help to tune the dielectric strength of the films, making them easier to form. More interestingly, the ability to tune the composition precisely enough so as to observe and continuously move through the percolative transition provides a good range of operation within which to implement TiO_x/TiO_y binary structures commonly used in resistive switches,[24,25] since the ideal barrier layer and injection layers would likely have oxygen deficiencies below and above the metal-insulator-transition.

The choice of a dimensionless state variable, in our case V^* the oxidation factor, is also far more useful independent variable than the typically employed oxygen flow rate. Aging of the target due to "race track" formation will subtly change the target area as well as its flux, making it difficult to get repeatable compositions. Due to the nonlinear relationship between oxygen flow rate and target oxidation, this can be

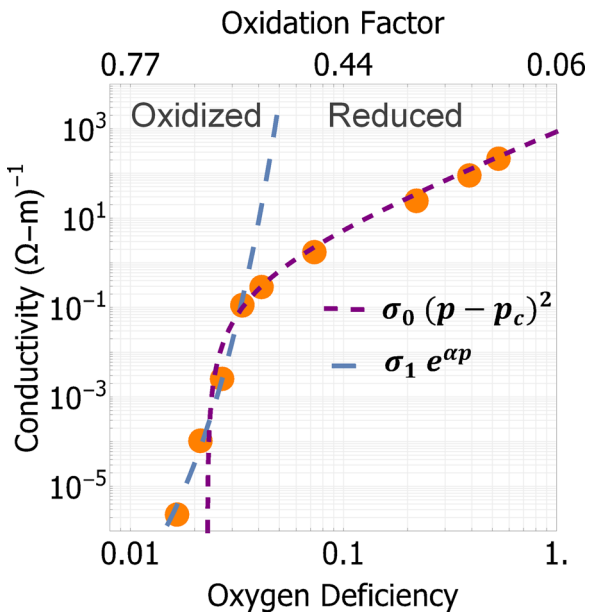

FIG. 3. (Color online) Coupled conductivity measurements and compositional fit with the equation of state from the simplified Berg model. Listed X-axis oxidation factors and oxygen deficiencies are calculated. Below the percolative threshold, the conductivity is modeled as an exponential. Above it is modeled as a classic percolative transition. "Oxidized" and "reduced" delimit corresponding regions in the supplementary material flow rate voltage diagram.

impossible to predict. The oxidation factor, however, being dimensionless would be more independent of these unintentional variations as well as introduced intentional variations, such as adjustment of the target power and growth rate. These effects can be tracked by periodically measuring ΔV_{max} and adjusting to the appropriate value of V^*.

IV. SUMMARY AND CONCLUSIONS

We have introduced the simplified Berg model as a reliable way to predict the composition of TiO_x in reactive sputtering. We showed that a dimensionless, process dependent quantity, the oxidation factor, can linearize the flux of Ti from the target. By coupling measured conductivity data to a predictive model of the composition, a classical percolative transition was observed. The low value of the critical concentration for percolation was attributed to the unique defect chemistry of reduced TiO_2. The implications for precise control of O:Ti ratio were also discussed in the context of resistive switching.

ACKNOWLEDGMENTS

The authors would like to thank Susanne Stemmer for helpful discussions and use of her sputter facilities. They would also like to thank Barry Wilkens for performing the relevant RBS measurements. This work was supported by the AFOSR MURI Grant No. FA9550-12-1-003. The research carried out here made use of x-ray facilities from the Materials Research Laboratory: an NSF MRSEC, supported by NSF-DMR 1121053. The authors gratefully acknowledge the use of RBS facilities within the LeRoy Eyring Center for Solid State Science at Arizona State University.

[1]S. Berg and T. Nyberg, Thin Solid Films **476**, 215 (2005).
[2]S. Berg, T. Larsson, C. Nender, and H. O. Blom, J. Appl. Phys. **63**, 887 (1988).
[3]D. Severin, O. Kappertz, T. Kubart, T. Nyberg, S. Berg, A. Pflug, M. Siemers, and M. Wuttig, Appl. Phys. Lett. **88**, 161504 (2006).
[4]S. Berg, E. Särhammar, and T. Nyberg, Thin Solid Films **565**, 186 (2014).
[5]W. D. Sproul, D. J. Christie, and D. C. Carter, Thin Solid Films **491**, 1 (2005).
[6]A. J. Lohn, J. E. Stevens, P. R. Mickel, and M. J. Marinella, Appl. Phys. Lett. **103**, 063502 (2013).
[7]J. E. Stevens, A. J. Lohn, S. A. Decker, B. L. Doyle, P. R. Mickel, and M. J. Marinella, J. Vac. Sci. Technol., A **32**, 021501 (2014).
[8]G. Buyle, D. Depla, K. Eufinger, J. Haemers, W. De Bosscher, and R. De Gryse, Vacuum **74**, 353 (2004).
[9]D. Depla, H. Tomaszewski, G. Buyle, and R. De Gryse, Surf. Coat. Technol. **201**, 848 (2006).
[10]D. Depla, S. Heirwegh, S. Mahieu, J. Haemers, and R. De Gryse, J. Appl. Phys. **101**, 013301 (2007).
[11]C. Jeynes, Z. H. Jafri, R. P. Webb, A. C. Kimber, and M. J. Ashwin, Surf. Interface Anal. **25**, 254 (1997).
[12]L. R. Doolittle, Instrum. Methods B **9**, 334 (1985).
[13]M. Mayer, AIP Conf. Proc. **475**, 541 (1999).
[14]D. Depla, S. Heirwegh, S. Mahieu, and R. De Gryse, J. Phys. D: Appl. Phys. **40**, 1957 (2007).
[15]D. Stauffer and A. Aharony, *Introduction to Percolation Theory* (Taylor & Francis, London and Bristol, PA, 1994).
[16]H. Stupp, M. Hornung, M. Lakner, O. Madel, and H. V. Löhneysen, Phys. Rev. Lett. **71**, 2634 (1993).
[17]L. A. Bursill and M. G. Blanchin, J. Phys. Lett. **44**, 165 (1983).
[18]L. A. Bursill, M. G. Blanchin, and D. J. Smith, Proc. R. Soc. London, Ser. A **391**, 373 (1984).
[19]M. G. Blanchin, L. A. Bursill, and D. J. Smith, Proc. R. Soc. London, Ser. A **391**, 351 (1984).
[20]E. J. Garboczi, K. A. Snyder, J. F. Douglas, and M. F. Thorpe, Phys. Rev. E **52**, 819 (1995).
[21]G. Ambrosetti, C. Grimaldi, I. Balberg, T. Maeder, A. Danani, and P. Ryser, Phys. Rev. B **81**, 155434 (2010).
[22]I. Balberg, J. Phys. D: Appl. Phys. **42**, 064003 (2009).
[23]S. Vionnet-Menot, C. Grimaldi, T. Maeder, S. Strässler, and P. Ryser, Phys. Rev. B **71**, 064201 (2005).
[24]J. J. Yang, F. Miao, M. D. Pickett, D. A. Ohlberg, D. R. Stewart, C. N. Lau, and R. S. Williams, Nanotechnology **20**, 215201 (2009).
[25]M. J. Lee *et al.*, Nat. Mater. **10**, 625 (2011).
[26]See supplementary material at http://dx.doi.org/10.1116/1.4974140 for a more detailed derivation of the simplified Berg model, more processing details, and Raman measurements.

Supplement to Maximizing Stoichiometry Control in Reactive Sputter Deposition of TiO_2

B.D. Hoskins and D.B. Strukov

Department of Electrical and Computer Engineering, University of California, Santa Barbara

I. Simplified Berg Model equation of state

The Berg model of reactive sputter deposition can be well described by two coupled equations relating growth rates and the composition[1].

$$\theta_2 = \frac{2\alpha_{cm}\left({}^{F}/_{R}\right)+Y_{oxide}\theta_1\left({}^{A_t}/_{A_f}\right)/(Y_{oxide}\theta_1+Y_{metal}(1-\theta_1))}{{}^{A_t}/_{A_f}+2\left({}^{F}/_{R}\right)(\alpha_{cmetal}-\alpha_{coxide})} \quad \text{(S1)}$$

$$R = F\frac{2(\alpha_{cmetal}-\theta_2(\alpha_{cmetal}-\alpha_{coxide}))}{\left({}^{A_t}/_{A_f}\right)\theta_2-S_N\theta_1\left({}^{A_t}/_{A_f}\right)/(Y_{oxide}\theta_1+Y_{metal}(1-\theta_1))} \quad \text{(S2)}$$

Where F is the flux of reactive gas, R is the flux of metal, θ_1 is the fraction reacted of the target, θ_2 is the fraction reacted of the film, α_{cmetal} is the sticking coefficient of gas to metal, α_{coxide} is the sticking coefficient of gas to compound, A_t and A_f are the effective target and film areas, and Y_{oxide} and Y_{metal} are the sputter yields of compound and metal. Equations S1 and S2 are the governing equation in the Berg model relating the target composition to the film growth, and it implies that continuous control over the target oxidation leads to continuous control over the film stoichiometry. This equation can be simplified by making some assumptions, namely that the sticking coefficient of the metal is always 1, while the sticking coefficient of the reactive species on the compound is 0 but 1 on the metal. This leads to the simplified Berg model equation of state:

$$x_f = \frac{2x_t}{x_t + \left(\frac{Y_{oxide}}{Y_{metal}}\right)(2-x_t) + \left(\frac{Y_{oxide}}{Y_{metal}}\right)\left(\frac{A_f}{A_t}\right)\left(\frac{2-x_t}{x_t}\right)} \quad \text{(S3)}$$

where x_t is the departure from stoichiometry of the target and x_f is the departure from stoichiometry of the film. This simplified Berg relation provides the key for understanding reactive sputter deposition namely, that for small x_t:

$$x_f = 2\frac{Y_{metal}}{Y_{oxide}}\frac{A_t}{A_f}(x_t)^2 \quad \text{(S4)}$$

This relationship reveals that control of the thin film stoichiometry is principally quadratic, that is that it's possible to achieve very precise control over the departure from stoichiometry for nearly stoichiometric films. In terms of growth rate, it also means that it's possible to achieve a large change in the growth rate of the film at the cost of only a small change of the composition of the film. In the Berg model, maximal correspondence between theory and experiment will occur during conditions of perturbative oxygen flow. Under these conditions, in the limiting case where gas absorption through fully oxidized regions of the film can be neglected, the departure from stoichiometry will vary quadratically with the oxidation state of the target at small deviations as well as inversely with the collector:target (A_t/A_f) ratio. This latter ratio can be varied by increasing the effective collector area which can be easily achieved by increasing the target-sample distance. Substantially reduced targets at great distances, therefore, can generate small deviations from stoichiometry.

II. Summary of growth behavior

A brief comparison between partial and completely opened pump valves (Figure S1) showed that the hysteresis typically seen in a reactive sputter process could be eliminated by "pumping out"

the hysteresis. This continuous control over the discharge properties will translate into continuous control over the grown film composition.

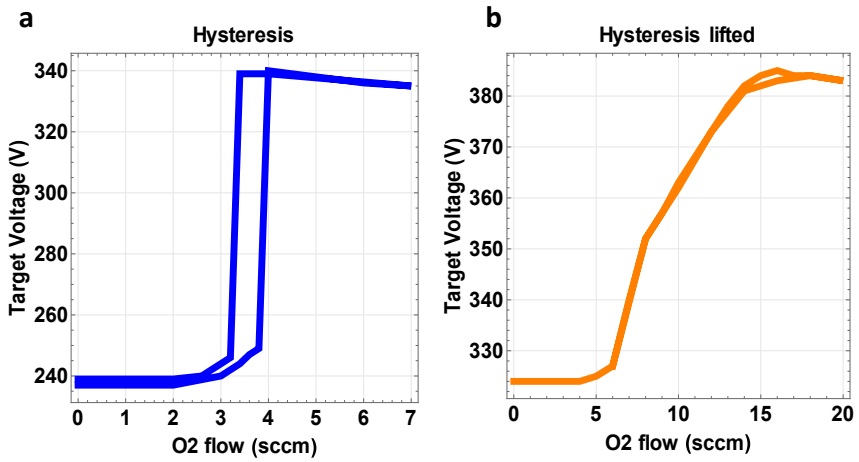

Figures S1. a) Hysteresis curve of the target voltage vs oxygen flow rate for a partially obstructed vacuum pump b) hysteresis free curve with a maximally pumped chamber.

By migrating to an alternative independent variable based on the target voltage, we can gain linear control over the Ti flux to the target. This linear control allows for continuous control over the material properties as can be seen from the relevant growth curves (Figure S2).

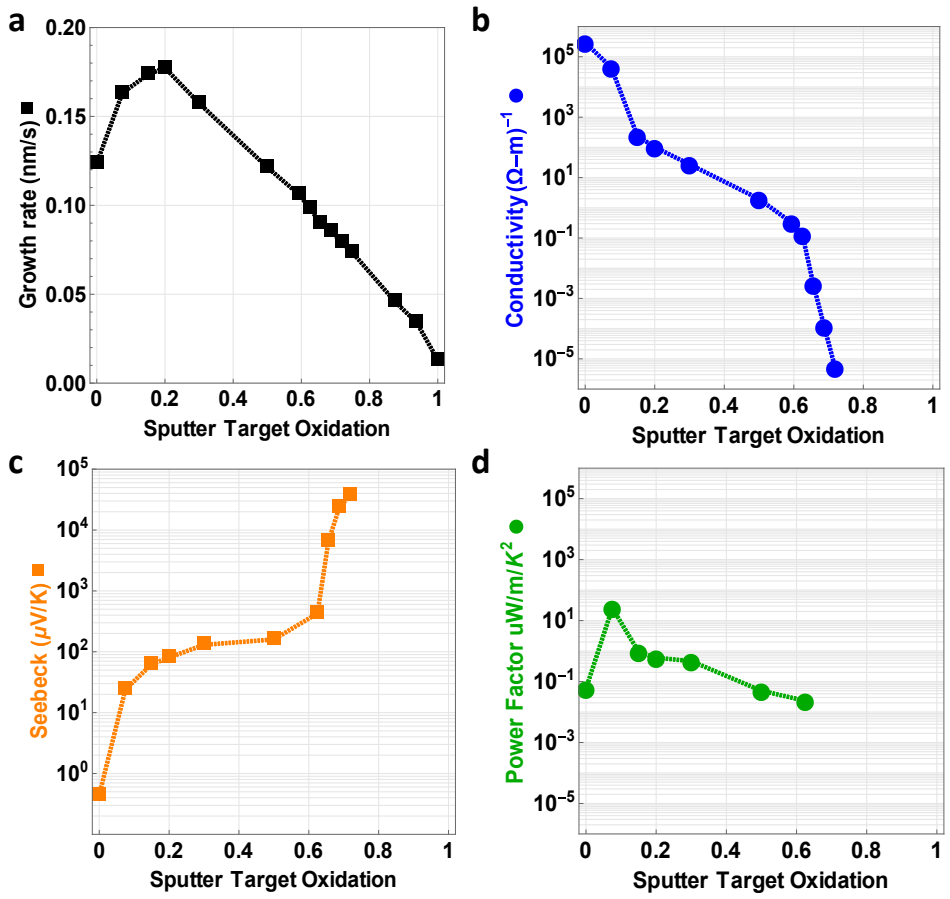

Figures S2 a) Growth rate of films as measured by XRR b) Van der Pauw measurement of 25-35 nm thick films c) Seebeck measurements of films from b d) measured power factor of films from b.

III. Suppression of Crystallinity

To investigate the microstructure of the films more explicitly, a third series of very thick films (~1μm) were grown on platinized silicon substrates. Extremely thin films are often found to be amorphous but later crystallize as the thickness increases[2]. Raman spectroscopy, which is a sensitive technique allowing for detection of both typical crystalline features, such as standard Raman Peaks, as well as amorphous features like the so-called Boson Peak [3, 4].

As can be seen in Figure S3, the thicker films corresponding to Oxidation Factor 1.0, or fully stoichiometric TiO_2 exhibit characteristic features of anatase. A move slightly off stoichiometry results in near complete suppression of the crystallinity with weak signal

generation corresponding to the second E_g signal at ~600 cm^{-1}. This weak signal is further suppressed as the film is reduced further at lower oxygen flow. Both factors 0.7 and 0.5 have a weak local maximum corresponding to the first E_g peak at around 100 cm^{-1}. The mixed valence state of Ti^{3+} and Ti^{4+} with their respective coordination differences is likely leading to the "confusion" effect often seen in mixed alloys as well as oxide glasses. These results suggest that crystallinity itself can be an indicator of stoichiometry in reduced TiO_2.

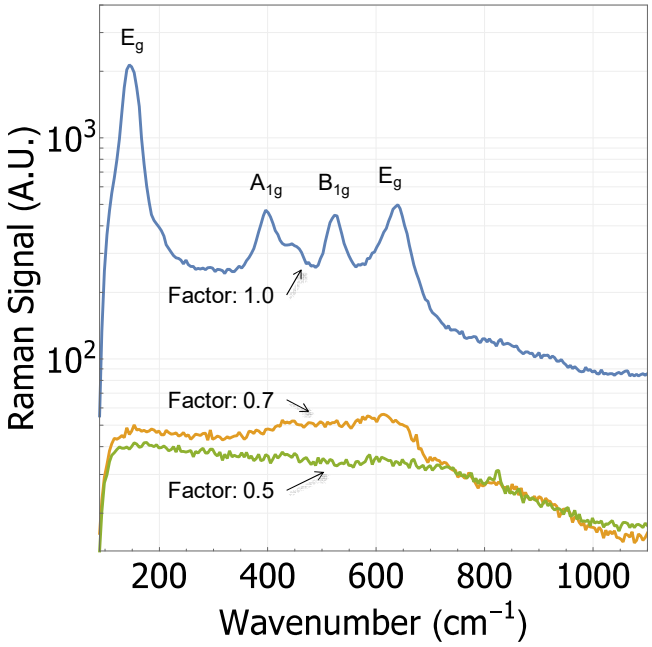

Figures S3. Effect of reduction on the crystallinity of 1µm thick films of TiO_x for films of oxidation factor 1.0, 0.7, and 0.5. Films grown under reducing conditions show a complete collapse in the film long range order.

1. Berg, S., et al., Predicting thin-film stoichiometry in reactive sputtering. Journal of Applied Physics, 1988. 63(3): p. 887.
2. Ohring, M., Materials Science of Thin Films. 2001: Elsevier Science.
3. Parker, J.C. and R.W. Siegel, Calibration of the Raman spectrum to the oxygen stoichiometry of nanophase TiO2. Applied Physics Letters, 1990. 57(9): p. 943.
4. Malinovsky, V.K. and A.P. Sokolov, The nature of boson peak in Raman scattering in glasses. Solid State Communications, 1986. 57(9): p. 757-761.